Supporting Information

Dual-functional metalloporphyrin-fluorenone covalent organic framework for solar hydrogen and oxygen production

Zhiwei Xiao,[a,b†] Huyue Wu,[a,b†] Lei Jiao,[b,d] Xiang Zhang,*[b,c,d] and Yaobing Wang*[b,c,d]

† These authors contributed equally to this work.

[a] College of Chemistry and Materials Science, Fujian Normal University, Fuzhou 350007, P. R. China.
[b] CAS Key Laboratory of Design and Assembly of Functional Nanostructures, and Fujian Provincial Key Laboratory of Nanomaterials, State Key Laboratory of Structural Chemistry, Fujian Institute of Research on the Structure of Matter, Chinese Academy of Sciences, Fuzhou 350002, Fujian, P. R. China.
E-mail: wangyb@fjirsm.ac.cn
[c] Fujian Science and Technology Innovation Laboratory for Optoelectronic Information of China, Fuzhou 350108, Fujian, P. R. China.
[d] University of Chinese Academy of Sciences, Beijing 100049, P. R. China

Supporting information for this article is given via a link at the end of the document.

Materials and methods

The meso-tetrakis (4-formylphenyl) porphyrin was purchased from Yao Ming Kand Pharmaceutical Co., Ltd., and 2,7-Diamino-9H-Fluoren-9-One was obtained from Yao MacLing Pharmaceutical Co., Ltd. Other reagents were acquired from China National Pharmaceutical Group Corporation (Sinopharm). Unless otherwise specified, the reagents do not require further purification.

Synthesis of Co-TFPP: Under stirring and a nitrogen atmosphere, meso-tetrakis(4-formylphenyl)porphyrin (TFPP, 50 mg, 0.069 mmol) and cobalt(II) acetate tetrahydrate ($Co(OAc)_2 \cdot 4H_2O$, 34.4 mg, 0.138 mmol) were dissolved in N,N-dimethylformamide (DMF, 20 mL) at 170 ℃ for 4 hours. After cooling and addition of water, the precipitate was filtered, washed with methanol, and vacuum-dried, yielding dark red Co-TFPP.

Synthesis of Co-TFPP-COF: Co-TPFO-COF was synthesized by reacting Co-TFPP (39.4 mg, 0.5 mmol) with 2,7-Diamino-9H-Fluoren-9-One (FOO) (21.0 mg, 1.0 mmol) in the presence of 6M acetic acid (0.5 mL) in a solution of 6 mL of o-dichlorobenzene: n-butanol = 1:1. The resulting mixture was loaded into a 10 mL Pyrex tube and subjected to ultrasound treatment for 10-15 minutes for uniform dispersion. The tube was then rapidly frozen at 77K (liquid nitrogen bath) and subjected to three freeze-pump-thaw cycles for degassing. The tube was sealed under vacuum and heated at 120 °C for 2 days. After the reaction, the precipitate was filtered, washed with tetrahydrofuran, DMF, and methanol, vacuum-dried at 60 °C for 12 hours, resulting in a deep brown powder.

Characterization

The PXRD (powder X-ray diffraction) patterns of the samples were recorded on an X-ray diffractometer with Cu-Kα radiation (D8 Advance, Bruker Ltd., Germany). Fourier-transform infrared (FTIR) spectra were recorded on a TENSOR 27 spectrometer (Bruker Ltd., Germany). UV-visible diffuse reflectance spectroscopy (UV-Vis-DRS) was performed using a PerkinElmer Lambda 950 spectrophotometer. The samples were sonically dispersed in ethanol, excited by a 400nm pump light, and subjected to femtosecond transient absorption (fs-TA) measurements using a femtosecond Ti: Sapphire regenerative amplifier (Ti: Sapphire laser system) and the Helios model ultrafast system.

Photoelectrochemical measurement

The transient photocurrent response, Mott-Schottky plots, Linear Sweep Voltammetry (LSV), and impedance were recorded using an electrochemical station (CHI 660E). A three-electrode electrochemical cell was employed with a Pt rod as the working electrode, a saturated Ag/AgCl reference electrode, and a 0.2 M Na_2SO_4 electrolyte. The working electrode ink consisted of 2 mg catalyst and 20 μL Nafion solution (5 wt.%) dispersed in 500 μL isopropanol, sonicated for 15 minutes to obtain a homogeneous slurry. The slurry was then coated onto a 1.0×2.5 cm2 fluorine-doped tin oxide (FTO) glass substrate, dried, resulting in the fabrication of the working electrode.

Photocatalytic performance for hydrogen evolution

The overall water splitting photocatalytic reaction was conducted using Perfect Light (Labsolar 6A) in a Pyrex-topped irradiation reaction vessel. In each reaction, 5 mg of photocatalyst was dispersed in a 100 ml solution of ascorbic acid (0.1 M). The suspension was deoxygenated by circulating through a cooling water system and maintained at 10°C. A xenon lamp, equipped with a long-pass filter ($\lambda > 420$ nm), was employed as the light source. Argon (Ar) was used as the carrier gas, and product analysis was performed using an online 9790 gas chromatograph (Agilent). After the photocatalytic experiment, the photocatalyst was washed with water and methanol, collected, and then vacuum-dried at 60°C.

Photocatalytic performance for oxygen evolution

Typically, 5 milligrams of photocatalyst are dispersed in 100 milliliters of water, using a 50 mM AgNO3 solution as the sacrificial agent. These photocatalytic reactions involve the generation of hydrogen gas and oxygen gas. The experimental setup and conditions are similar to the above-mentioned photocatalytic reactions, with the only difference being the sacrificial agent used.

AQY determination

Under 300W xenon lamp irradiation, the apparent quantum yields (AQY) of hydrogen and oxygen evolution were measured using different bandpass filters. The AQY values were calculated using the following equation (1):

$$\begin{aligned} AQY(\%) &= \frac{\text{number of incident obtaine}}{\text{number of incident photon}} \times 100\% \\ &= \frac{10^9(\nu \times N_A \times K) \times (h \times c)}{(I \times A \times \lambda)} \times 100\% \\ &= \frac{1.2 \times 10^8(\nu \times K)}{(I \times A \times \lambda)} \times 100\% \end{aligned} \quad (1)$$

where ν is the reaction rate (mol s^{-1}), N_A is the Avogadro constant (6.022×10^{23} mol^{-1}), K is the number of electrons transferred in the reaction, h is Planck's constant (6.626×10^{-34} J s), c is the speed of light (3.0 x 10 m s^{-1}) , I is the optical power density (W m^2), A is the area of incident light (m^2) , λ is the wavelength (nm).

DFT methods

Under the Generalized Gradient Approximation (GGA), single-point energy calculations were performed using the spin-polarized Perdew-Burke-Ernzerhof (PBE) functional within the Vienna Ab-initio Simulation Package (VASP). To avoid artificial interactions between periodic images, a 10 Å vacuum layer perpendicular to the thin slab was added. Brillouin zone integration was carried out using a 1 × 1 × 1k-point grid. The free energy change (ΔG) of reaction intermediates can be calculated using the following formula (2):

$$\Delta G = \Delta E + \Delta E_{ZPE} - T\Delta S \quad (2)$$

where ΔE is the adsorption energy on the cluster surface calculated using Density Functional Theory (DFT). ΔE_{zpe} and ΔS are differences in zero-point energy and entropy, respectively.

Supplementary figures

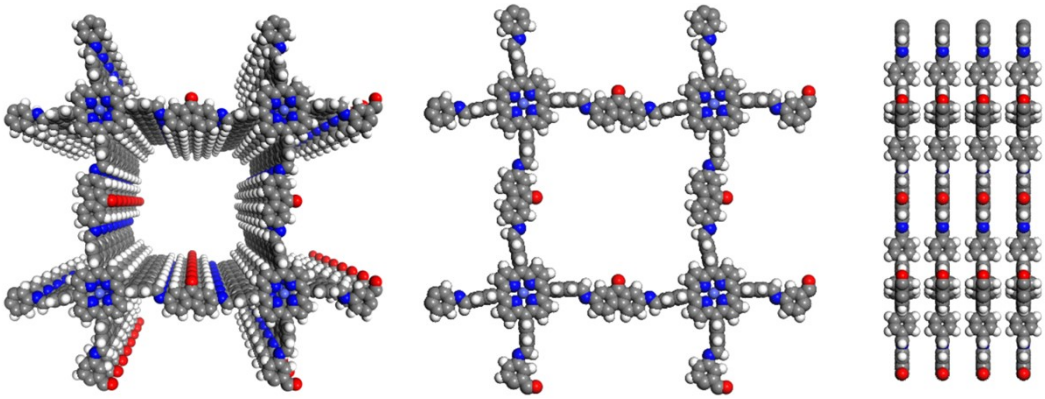

Figure S1. 3D structures of the AA stacking models of the Co-TPFO-COF (top and side view)

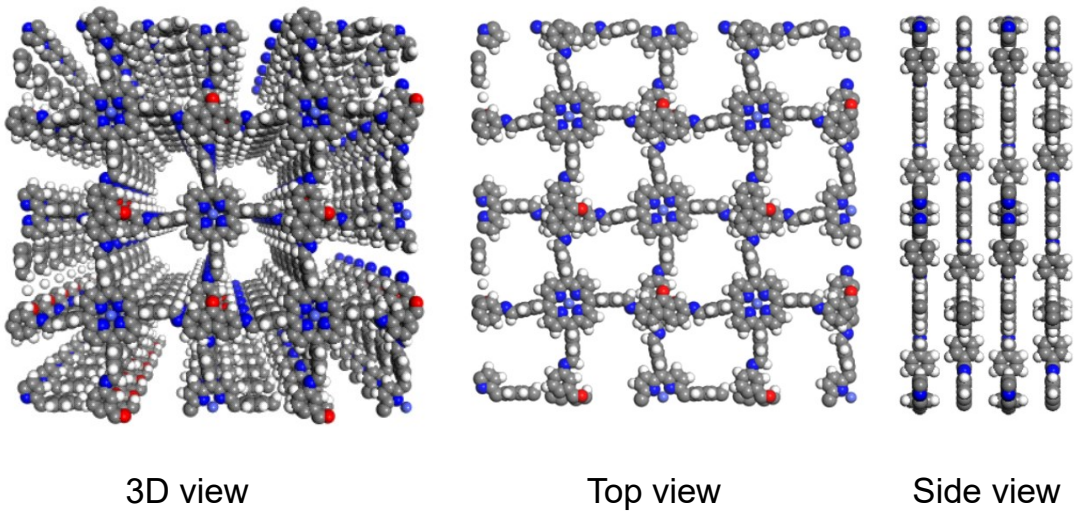

Figure S2. 3D structures of the AB stacking models of the Co-TPFO-COF (top and side view)

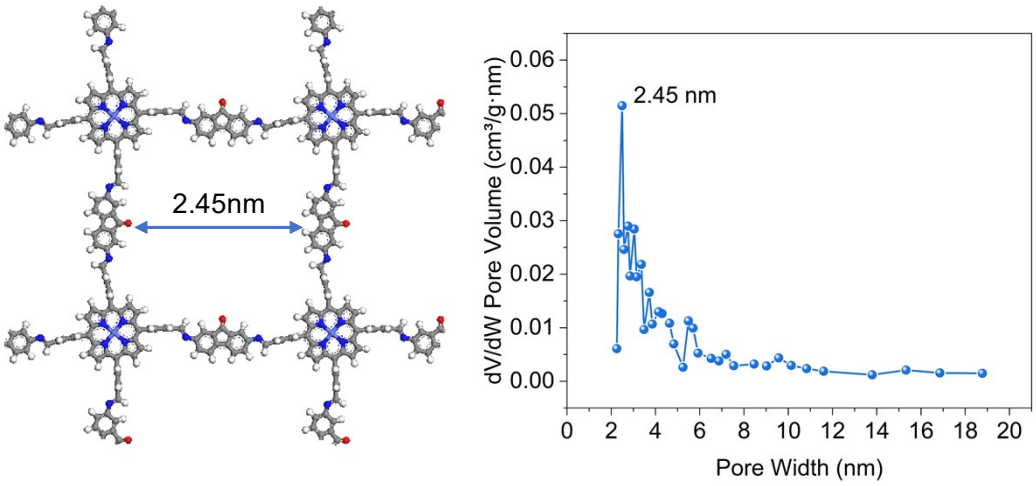

Figure S3. Consistency of pore size measured by BET test with simulation model.

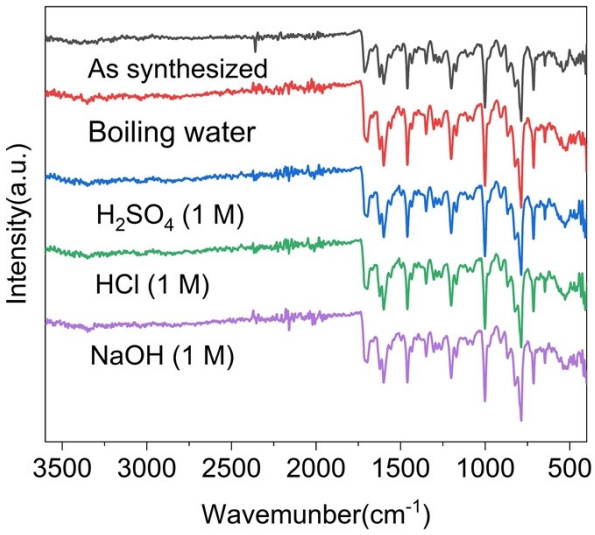

Figure S4. FT-IR spectra of Co-TFPP-COF after treatments under different chemical environments for 12 h.

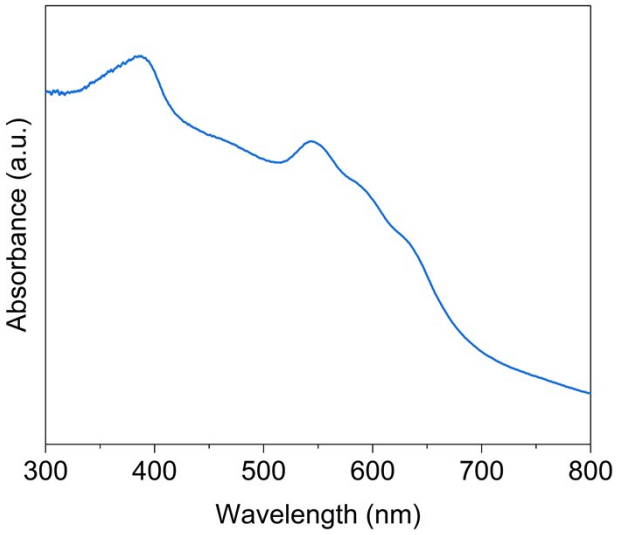

Figure S5. UV-Vis diffuse reflectance spectra of the Co-TFPP-COF.

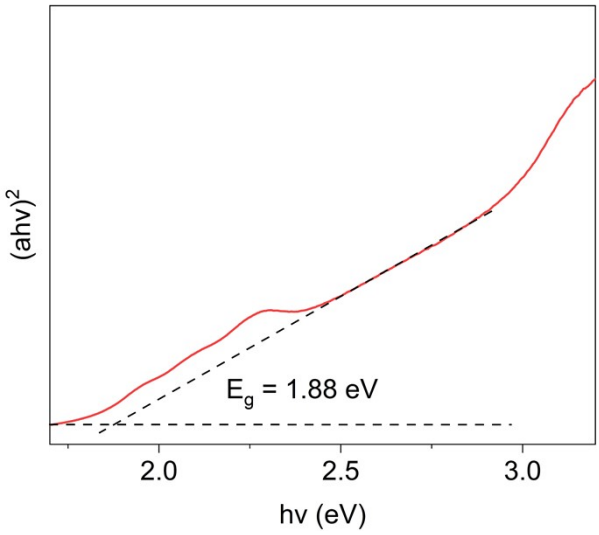

Figure S6. Tauc plots of the Co-TFPP-COF.

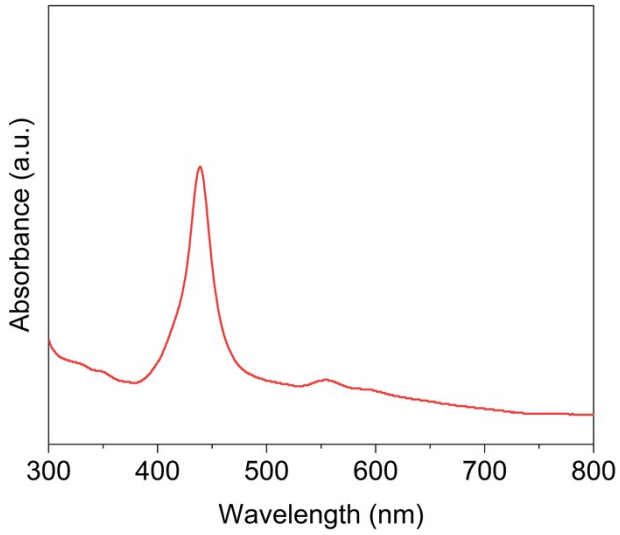

Figure S7. UV-Vis absorption spectroscopy on the water suspension of Co-TPFO-COF.

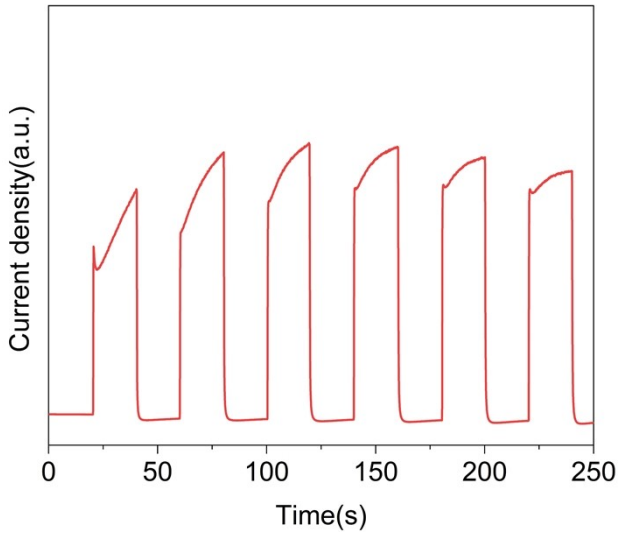

Figure S8. Transient photocurrents of Co-TFPP-COF under visible light irradiation.

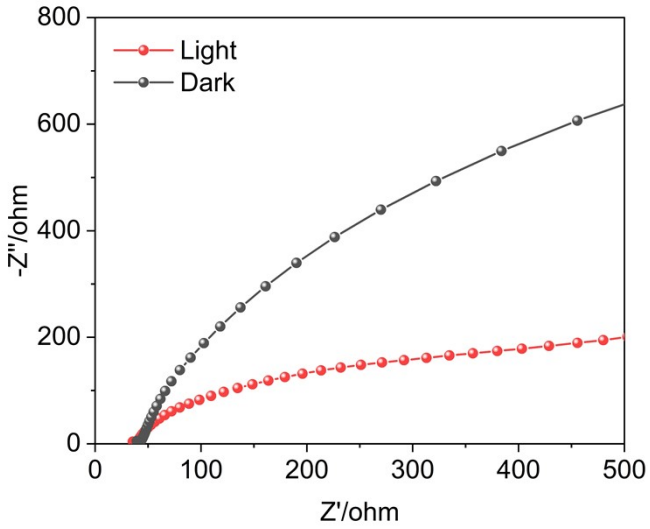

Figure S9. The Nyquist plots in dark and under light irradiation.

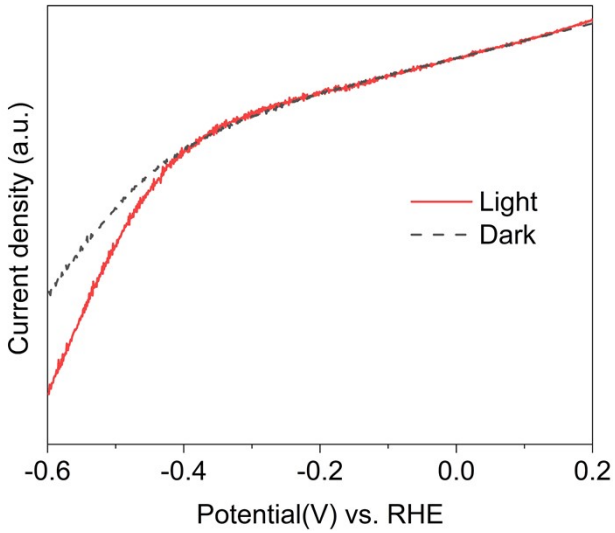

Figure S10. I−V curves in dark and under light irradiation for HER.

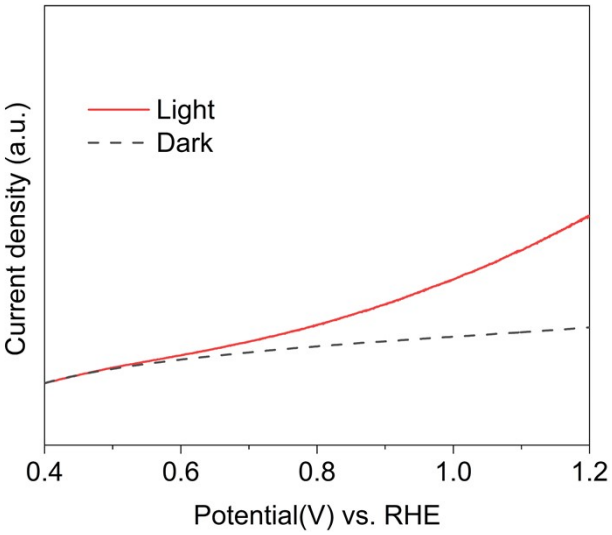

Figure S11. I−V curves in dark and under light irradiation for OER.

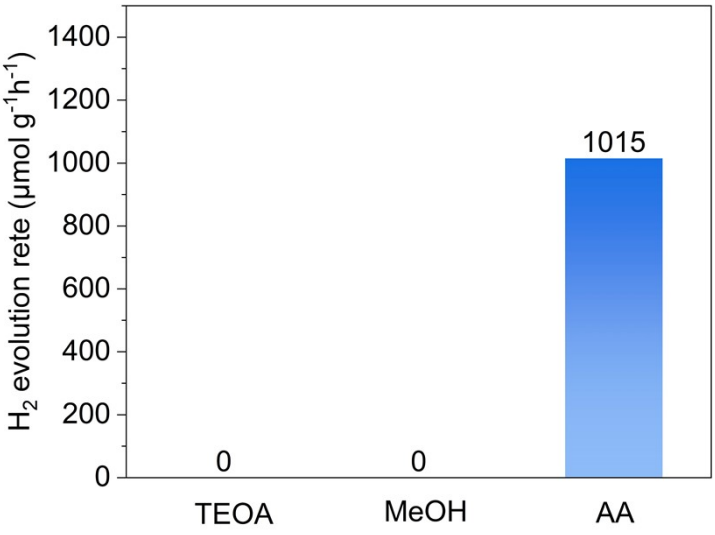

Figure S12. Hydrogen evolution rates under different sacrificial agent conditions.

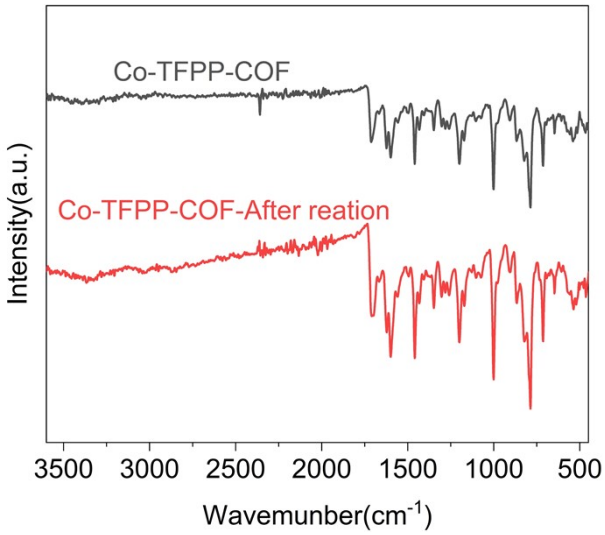

Figure S13. FT-IR spectra of Co-TFPP-COF as-synthesized and after long-term photocatalytic hydrogen evolution tests.

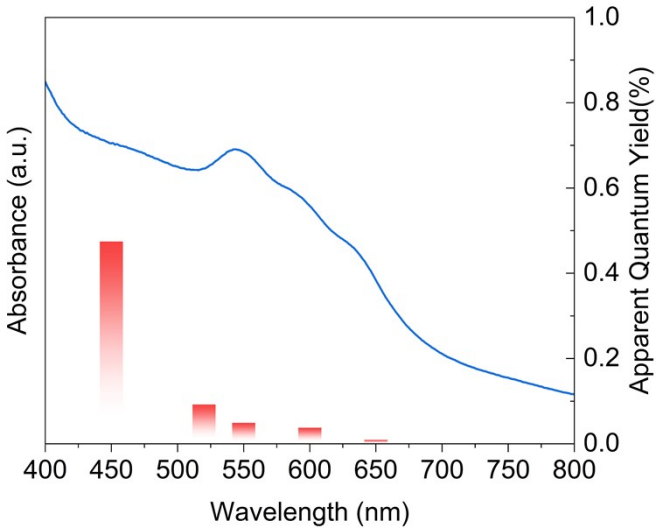

Figure S14. Wavelength-dependent quantum yield (AQY) for the photocatalytic hydrogen production of Co-TFPP-COF.

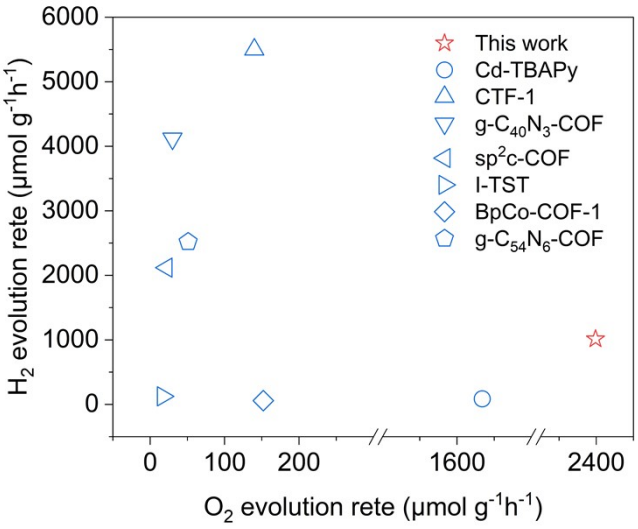

Figure S15. The comparison of photocatalytic water reduction and oxidation performances of reported dual-functional MOFs, CTFs and COFs photocatalysts.

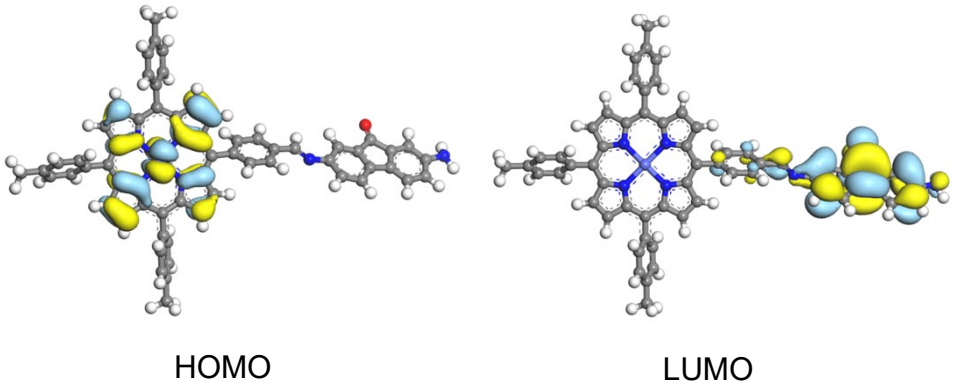

Figure S16. The distribution of LUMO and HOMO orbitals in the Co-TFPP-COF.

Table S1. Photocatalytic H_2 evolution performances of reported dual-functional MOFs, CTFs and COFs photocatalysts.

Catalysts	Co-catalyst	Irradiance	Sacrificial donor	H_2 evolution rate ($\mu mol\ g^{-1}\ h^{-1}$)	Reference
Co-TPFO-COF	3wt% Pt	⩾420 nm	AA	1015	This work
Cd-TBAPy	3.5wt% Pt	⩾420 nm	TEOA	86	[1]
CTF-1	2.01wt% Pt	⩾420 nm	AA	5500	[2]
g-$C_{40}N_3$-COF	3wt% Pt	⩾420 nm	AA	4120	[3]
sp^2c-COF	3wt% Pt	⩾420 nm	TEOA	2120	[4]
I-TST	3wt% Pt	⩾420 nm	TEOA	125	[5]
BpCo-COF-1	0.4wt% Pt	⩾420 nm	TEOA	59.4	[6]
g-$C_{54}N_6$-COF	3wt% Pt	⩾420 nm	TEOA	2519	[7]

Table S2. Photocatalytic O_2 evolution performances of reported dual-functional MOFs, CTFs and COFs photocatalysts.

Catalysts	Co-catalyst	Irradiance	Sacrificial donor	O_2 evolution rate ($\mu mol\ g^{-1}\ h^{-1}$)	Reference
Co-TPFO-COF	-	⩾420 nm	$AgNO_3$	2399	This work
Cd-TBAPy	0.4wt% Co	⩾420 nm	$AgNO_3$	1634	[1]
CTF-1	3wt% RuO_x	⩾420 nm	$AgNO_3$	140	[2]
g-$C_{40}N_3$-COF	3wt% Co	⩾420 nm	$AgNO_3$	30	[3]
sp^2c-COF	3wt% Co	⩾420 nm	$AgNO_3$	22	[4]
I-TST	3wt% Co	⩾420 nm	$AgNO_3$	17	[5]
BpCo-COF-1	2.5wt% Co	⩾420 nm	$AgNO_3$	152	[6]
g-$C_{54}N_6$-COF	3wt% Co	⩾420 nm	$AgNO_3$	51	[7]

Table S3. Fractional atomic coordinates for crystal structure of Co-TPFO-COF.

Space group: *P6/m* a = 29.1261 Å , b = 28.9902 Å, c = 6.6902 Å α = β = 90.0000°, γ = 90.1194°			
Atom	x	y	z
C1	0.46432	0.71128	-0.1812
C2	0.45429	0.75841	-0.18113
C3	0.67613	0.53943	0.1812
C4	0.7241	0.54104	0.18114
C5	0.5037	0.33218	0.18131
C6	0.50549	0.284	0.18121
C7	0.29863	0.49875	-0.1813
C8	0.25172	0.48845	-0.1811
H9	0.46729	0.69304	-0.32161
H10	0.44955	0.77625	-0.32162
H11	0.65777	0.53829	0.32163
H12	0.74248	0.54111	0.32166
H13	0.50241	0.35051	0.32206
H14	0.50564	0.26562	0.32203
H15	0.31667	0.5018	-0.32206
H16	0.23396	0.48361	-0.32159
C17	0.3797	0.42599	0
C18	0.41542	0.39685	0
C19	0.4546	0.42398	0
N20	0.44493	0.47	0
C21	0.39809	0.47008	0
C22	0.39207	0.62733	0
C23	0.36286	0.5914	0
C24	0.38971	0.55207	0
N25	0.43556	0.56179	0
C26	0.43581	0.60881	0
C27	0.37058	0.50866	0
C28	0.59223	0.61539	0
C29	0.5564	0.6446	0
C30	0.51734	0.61742	0
N31	0.52697	0.57143	0
C32	0.57378	0.57139	0
C33	0.47422	0.63641	0
C34	0.5801	0.41424	0
C35	0.60914	0.45032	0
C36	0.58213	0.4895	0
N37	0.53634	0.47962	0
C38	0.53625	0.43256	0

C39	0.49783	0.40485	0
C40	0.60115	0.53292	0
C41	0.46872	0.6874	0
C42	0.65199	0.5381	0
C43	0.50261	0.3565	0
C44	0.32246	0.50338	0
C45	0.44878	0.78197	0
C46	0.7482	0.54135	0
C47	0.50622	0.25976	0
C48	0.22827	0.48277	0
C49	0.79841	0.53938	0
C50	0.50555	0.21199	0
N51	0.14704	0.49591	0
N52	0.81832	0.49937	0
C53	0.0345	0.42976	0
C54	0.08188	0.43879	0
C55	0.09877	0.48496	0
C56	0.06732	0.52186	0
C57	0.00449	0.46701	0
C58	0.02047	0.51191	0
C59	0.98772	0.54267	0
C60	0.86679	0.49012	0
C61	0.88066	0.44356	0
C62	0.92998	0.43156	0
C63	0.96118	0.46783	0
C64	0.94685	0.51331	0
C65	0.9005	0.52548	0
N66	0.46352	0.86502	0
N67	0.46458	0.18976	0
C68	0.39692	0.97628	0
C69	0.40488	0.92871	0
C70	0.45328	0.91077	0
C71	0.48959	0.94283	0
C72	0.43452	1.00591	0
C73	0.47928	0.98979	0
C74	0.51006	0.0228	0
C75	0.45687	0.14348	0
C76	0.41069	0.12823	0
C77	0.39979	0.08106	0
C78	0.43567	0.04946	0
C79	0.48096	0.06377	0
C80	0.49277	0.11042	0
C81	0.43291	0.82979	0
C82	0.18066	0.46657	0

O83	0.55187	0.02204	0
O84	0.98854	0.58468	0
Co85	0.48594	0.5207	0
H86	0.34392	0.41576	0
H87	0.41282	0.35958	0
H88	0.38211	0.66328	0
H89	0.32578	0.59392	0
H90	0.62804	0.62547	0
H91	0.55886	0.68187	0
H92	0.59014	0.3783	0
H93	0.64624	0.4479	0
H94	0.81756	0.5713	0
H95	0.53789	0.19385	0
H96	0.02175	0.39465	0
H97	0.10456	0.40945	0
H98	0.07918	0.55728	0
H99	0.85526	0.41622	0
H100	0.94113	0.39597	0
H101	0.8916	0.5616	0
H102	0.36224	0.98958	0
H103	0.3754	0.90614	0
H104	0.52499	0.93144	0
H105	0.38306	0.15317	0
H106	0.36437	0.06969	0
H107	0.52865	0.11982	0
H108	0.39632	0.83541	0
H109	0.17505	0.42977	0

References

[1] Y. Xiao, Y. Qi, X. Wang, X. Wang, F. Zhang, C. Li, *Adv. Mater.* **2018**, *30*, e1803401.

[2] J. Xie, S. A. Shevlin, Q. Ruan, S. J. A. Moniz, Y. Liu, X. Liu, Y. Li, C. C. Lau, Z. X. Guo, J. Tang, *Energy Environ. Sci.* **2018**, *11*, 1617-1624.

[3] S. Bi, C. Yang, W. Zhang, J. Xu, L. Liu, D. Wu, X. Wang, Y. Han, Q. Liang, F. Zhang, *Nat. Commun.* **2019**, *10*, 2467.

[4] E. Jin, Z. Lan, Q. Jiang, K. Geng, G. Li, X. Wang, D. Jiang, *Chem* **2019**, *5*, 1632-1647.

[5] J. Chen, X. Tao, C. Li, Y. Ma, L. Tao, D. Zheng, J. Zhu, H. Li, R. Li, Q. Yang, *Appl. Catal. B Environ.* **2020**, *262*, 118271.

[6] Y. Wan, L. Wang, H. Xu, X. Wu, J. Yang, *J. Am. Chem. Soc.* **2020**, *142*, 4508-4516.

[7] J. Xu, C. Yang, S. Bi, W. Wang, Y. He, D. Wu, Q. Liang, X. Wang, F. Zhang, *Angew. Chem. Int. Ed. Engl.* **2020**, *59*, 23845-23853.